Research Article

Azzh Saad Alshehry, Humaira Yasmin*, Abdul Hamid Ganie, and Rasool Shah

Heat transfer performance of magnetohydrodynamic multiphase nanofluid flow of $Cu–Al_2O_3/H_2O$ over a stretching cylinder

https://doi.org/10.1515/phys-2023-0142
received August 29, 2023; accepted October 25, 2023

Abstract: This study examines the heat transfer properties of a recently created hybrid nanofluid in contrast to a traditional nanofluid. The aim is to improve the transfer of heat in the flow of the boundary layer by employing this novel hybrid nanofluid. Our study investigates the impact of the Lorentz force on a three-dimensional stretched surface. We utilize a new model that incorporates thermophysical factors. A quantitative parametric study is performed to investigate the influence of different physical parameters, enabling meaningful comparisons. The results demonstrate that the hybrid nanofluid exhibits a higher heat transfer rate compared to the conventional fluid, even in the presence of a magnetic field. Moreover, the efficiency of heat transfer can be enhanced by modifying the concentration of nanoparticles in the hybrid nanofluid.

Keywords: hybrid nanofluid, stretching cylinder, magnetohydrodynamics, Haar wavelet collocation method

1 Introduction

Researchers have shown that some liquid coolants have significantly lower thermal conductivities than solid metals. Several technical and industrial processes rely on the efficiency and effectiveness of natural laminar and convective thermal energy transmission. A wide variety of technical and technological applications for the recently produced fluid known as hybrid nanofluid; "when two kinds of nanoparticles are mixed in one liquid, the result is called a hybrid nanofluid."

Consequently, while selecting materials for nanoparticles, complementing each other is essential [1–3]. Nanoparticles of metals like aluminum, copper, and zinc are excellent thermal conductors. Unfortunately, these metallic nanoparticles' reactivity and stability restrict their usage in nanofluid applications [4]. On the other hand, ceramic nanoparticles offer several advantageous properties but a poorer thermal conductivity than metal nanoparticles [5–7].

It has also been proven that increasing the carrier fluid's thermal conductivity is the primary goal of incorporating nanomaterials into carrier fluids. It is also observed that stable nanofluids have notable features, such as increased heat conductivity rate with low concentrations of nanoparticles. Several studies [8–11] have been conducted to understand better how to improve thermal conductivity and thermal performances using a single nanomaterial. Recent experimental and numerical efforts on nanofluids/hybrid nanofluids have shown that these materials significantly improve heat transmission compared to traditional liquids. The fluid dynamics properties are analyzed in light of the impact of various intriguing factors [12–15].

The copper-alumina ($Cu-Al_2O_3$) nanocomposite powder was manufactured by Suresh *et al.* [16] using a thermochemical approach, and a hybrid nanofluid was generated using a two-step method. In another study, Suresh *et al.* [17] performed the heat transport analysis of a $Cu–Al_2O_3/H_2O$ hybrid nanofluid. They [18] also examined the heat transfer and pressure drop characteristics of a dilute copper–alumina/water ($Cu–Al_2O_3/H_2O$) hybrid nanofluid flow. Momin [19] studied the combined convection laminar flow of the $Cu–Al_2O_3/H_2O$ nanofluid across an angled tube.

The heat transport properties of (Fe_3O_4)/grapheme hybrid nanofluid were experimentally investigated by Askari *et al.* [20]. A differentially heated porous cavity

* **Corresponding author: Humaira Yasmin,** Department of Basic Sciences, General Administration of the Preparatory Year, King Faisal University, Al-Ahsa, 31982, Saudi Arabia, e-mail: hhassain@kfu.edu.sa
Azzh Saad Alshehry: Department of Mathematical Sciences, Faculty of Sciences, Princess Nourah Bint Abdulrahman University, P. O. Box 84428, Riyadh 11671, Saudi Arabia, e-mail: asalshihry@pnu.edu.sa
Abdul Hamid Ganie: Basic Science Department, College of Science and Theoretical Studies, Saudi Electronic University, Riyadh 11673, Saudi Arabia, e-mail: a.ganie@seu.edu.sa
Rasool Shah: Department of Mathematics, Abdul Wali Khan University, Mardan 23200, Pakistan, e-mail: shahrasool26@gmail.com

with a free convection flow of combined nanofluids was investigated by Mehryan *et al.* [21]. For the porous matrix, they studied aluminum metal foam and glass balls. According to the data, hybrid nanofluids have improved dynamic viscosity and thermal conductivity. Benzema *et al.* [22] employed a computational method to investigate the evolution of entropy in an Ag–MgO/H_2O hybrid nanofluid subjected to random heating and venting. The findings show that the thickening of the thermal interface close to the heated walls is reduced as the strength of the magnetic field increases. When nanoparticles are mixed into a base fluid, the entropy of the system tends to increase. Sundar *et al.* [23] conducted an experiment to measure the Darcy–Weisbach friction factor and convective coefficient of a multiwall carbon hybrid nanofluid moving in a fully developed turbulent flow inside a uniformly heated circular tube. Forced convective heat transfer was investigated by Labib *et al.* [24] using a computational method to assess the effect of the carrier fluid and hybrid nanofluid. The literature contains recent experiments [25–28] that provide a detailed examination of the flow behavior of nanofluids, considering various features. The Haar wavelet collocation method [29–32] has been used to compute the nonlinear governing systems. The fluid flow characteristics are examined due to the effects of several intriguing variables.

The research articles in this collection investigate soliton solutions in various fractional models using a range of mathematical techniques. Yasmin, Aljahdaly, Saeed, and Shah's research aims to comprehend optical soliton solutions in coupled systems, birefringent fibers, and fractionally perturbed models. To study families of soliton solutions in these intricate models, they use an enhanced direct algebraic method and cutting-edge analytical tools. Additionally, they studied symmetric soliton solutions in the Konno–Onno system [33–35]. Furthermore, a comparative analysis of advection–dispersion equations with Atangana–Baleanu fractional derivatives and a numerical analysis of the Belousov–Zhabotinsky system are provided by contributions from previous study. Furthermore, the analytical evaluation of time-fractional Fisher's equations is the main emphasis of Zidan, Khan, Alaoui, and Weera. Finally, using novel methods, Mukhtar, Shah, and Noor conducted a numerical study of a fractional-order multi-dimensional Navier–Stokes equation. These studies, through numerical and analytical investigations, add to the comprehensive understanding of soliton solutions in different fractional models [36–38].

2 Mathematical formulation

This study investigates the hydromagnetic flow of alumina–copper/water hybrid nanofluids *via* a permeable stretch

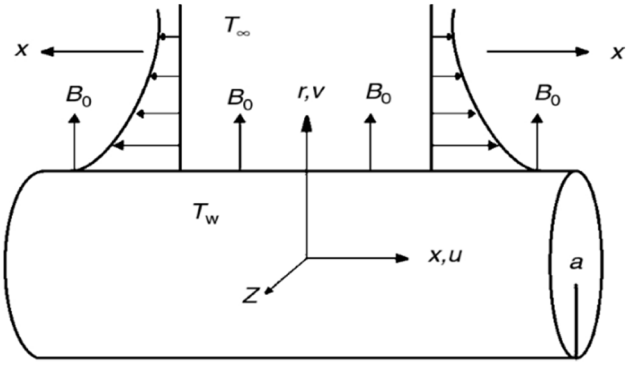

Figure 1: Schematic diagram for flow geometry.

cylinder under stable and incompressible boundary layer conditions. A magnetic field is applied from the outside. When the elastic cylinder is stretched, the flow of the hybrid nanofluid is modified along its axial axis. Using a coordinate system in which (x, r) denotes the axial and radial directions, as the elongating cylinder moves along its axis, we can start a flow of fluid. Figure 1 shows the geometrical variables and schematic coordinates of the flow.

To express the conservation rules of energy, mass, and momentum in the boundary layer approximation with boundary conditions, we have

$$\frac{\partial}{\partial x}(ru) + \frac{\partial}{\partial r}(rv) = 0, \tag{1}$$

$$\rho_h\left[u\frac{\partial u}{\partial x} + v\frac{\partial u}{\partial r}\right] = \frac{\mu_h}{r}\frac{\partial}{\partial r}\left(r\frac{\partial u}{\partial r}\right) - \sigma B_\circ^2 u + (\rho\beta)_h(gT - gT_\infty), \tag{2}$$

$$[\rho c_p]\left(u\frac{\partial}{\partial x}(T) + v\frac{\partial}{\partial r}(T)\right) = k_h r\left(\frac{\partial^2 u}{\partial r^2}\right) - \frac{\partial^2 Q}{\partial r} + \mu_h\left(\frac{\partial u}{\partial r}\right)^2 + \sigma B_0^2 u^2, \tag{3}$$

$$r \to a, \quad u = cx, \quad v = 0, \quad T \to T_w, \tag{4}$$

$$r \to \infty, \quad u = 0, \quad T \to T_\infty. \tag{5}$$

The following is the Rosseland flux model for the investigation of electromagnetic radiation:

$$Q = -\frac{\partial T^4}{\partial r}\frac{4\sigma}{3k}. \tag{6}$$

The series expansion method yields

$$T^4 = 4T_\infty^3 T - 3T_\infty^4, \tag{7}$$

$$\frac{\partial Q}{\partial r} = -\frac{16\sigma T_\infty^3}{3k}\frac{\partial^2 T}{\partial r^2}. \tag{8}$$

To reduce the model equations to a dimensionless form, we use the following transformations:

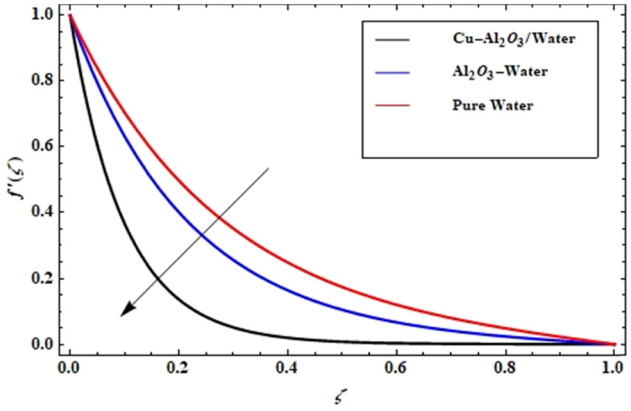

Figure 2: Particle concentration *versus* $f'(\zeta)$.

$$\zeta = \frac{r^2 - a^2}{2a}\left(\frac{c}{a}\right)^{1/2}, \quad u = cx\frac{\partial F}{\partial \zeta}, \quad v = -\frac{a}{r}(cv)^{1/2}F(\zeta), \theta(\zeta) = \frac{T - T_\infty}{T_w - T_\infty}. \tag{9}$$

We obtain the following equations by plugging these coordinates into Eqs. (2)–(5), with Eq. (1) being satisfied uniquely:

$$A_1\left[(1 + 2\zeta\gamma)\frac{\partial^3 F}{\partial \zeta^3} + 2\gamma\frac{\partial^2 F}{\partial \zeta^2}\right] + A_2\left[F\frac{\partial^2 F}{\partial \zeta^2} - \left(\frac{\partial F}{\partial \zeta}\right)^2\right] - M\left(\frac{\partial F}{\partial \zeta}\right) + A_3\lambda\theta = 0, \tag{10}$$

$$\left[(A_4 + Rd)(1 + 2\zeta\gamma)\frac{\partial^2 \theta}{\partial \zeta^2}\right] + (2A_4 + \mathrm{Rd})\gamma\frac{\partial \theta}{\partial \zeta} + \mathrm{EcPr}\left[M\left(\frac{\partial F}{\partial \zeta}\right) + A_1(1 + 2\zeta\lambda)\left(\frac{\partial F}{\partial \zeta}\right)^2\right], \tag{11}$$

$$F_{\zeta=0} = 0, \quad \left(\frac{\partial F}{\partial \zeta}\right)_{\zeta=0} = 1, \quad \theta_{\zeta=0} = 1, \tag{12}$$

$$\left(\frac{\partial F}{\partial \zeta}\right)_{\zeta\to 0} = 0, \quad \theta_{\zeta\to\infty} = 0. \tag{13}$$

Eqs. (10) and (11) are the governing equations and involve several dimensionless parameters in which $\lambda = \frac{\mathrm{Gr}}{\mathrm{Re}^2}$, $M = \frac{\sigma B_*^2}{c\rho_f}$, $\gamma = \left(\frac{v}{ca^2}\right)^{1/2}$, $\mathrm{Rd} = \frac{16\sigma T_\infty^3}{3kk_f}$ represent convection, magnetic, curvature, and radiation parameters, respectively, where local Reynolds number, Grashof number, Eckert number, and Prandtl number are represented by $\mathrm{Re} = \frac{cx^2}{v}$, $\mathrm{Gr} = \frac{g\beta(T_w - T_\infty)x^3}{v^3}$, $\mathrm{Ec} = \frac{U_w^2}{(cp)_f(T_w - T_\infty)}$, $\mathrm{Pr} = \frac{\mu_f c_p}{k_f}$, respectively.

As mentioned earlier, the constant terms can be written as

$$A_1 = \frac{\mu_{\mathrm{hf}}}{\mu_{\mathrm{cf}}}, \quad A_2 = \frac{\rho_{\mathrm{hf}}}{\rho_{\mathrm{cf}}}, \quad A_3 = \frac{(\rho\beta)_{\mathrm{hf}}}{(\rho\beta)_{\mathrm{cf}}}, \quad A_4 = \frac{k_{\mathrm{hf}}}{k_{\mathrm{cf}}}, \quad A_5 = \frac{(\rho c_p)_{\mathrm{hf}}}{(\rho c_p)_{\mathrm{cf}}}. \tag{14}$$

According to previous studies [12], the hybrid nanofluid's properties, including its heat capacity, are described as follows:

$$\rho_{\mathrm{hf}} = (1 - \vartheta_{n_2})[(1 - \vartheta_{n_2})\rho_f + \vartheta_{n_1}\rho_{n_1}] + \vartheta_{n_2}\rho_{n_2}, \tag{15}$$

$$\mu_{\mathrm{hf}} = \mu_{\mathrm{cf}}(1 - \vartheta_{n_1})^{-2.5}(1 - \vartheta_{n_2})^{-2.5}, \tag{16}$$

$$(\rho_{cp})_{hf} = (1 - \vartheta_{n_2})[(1 - \vartheta_{n_1})(\rho c_p)_f + \vartheta_{n_1}(\rho c_p)_{n_1}] + \vartheta_{n_2}(\rho c_p)_{n_2}, \tag{17}$$

$$(\rho\beta)_{hf} = (1 - \vartheta_{n_2})[(1 - \vartheta_{n_1})(\rho\beta)_f + \vartheta_{n_1}(\rho\beta)_{n_1}] + \vartheta_{n_2}(\rho\beta)_{n_2}, \tag{18}$$

$$\frac{k_{\mathrm{hf}}}{k_{\mathrm{cf}}} = \frac{k_{n_2} + (m - 1)k_{\mathrm{cf}} - (m - 1)\vartheta_{n_2}(k_{\mathrm{cf}} - k_{n_2})}{k_{n_2} + (m - 1)k_{\mathrm{cf}} + \vartheta_{n_2}(k_{\mathrm{cf}} - k_{n_2})}, \tag{19}$$

$$\frac{k_{\mathrm{nf}}}{k_{\mathrm{cf}}} = \frac{(m - 1)k_{\mathrm{cf}} + k_{n_1} - (m - 1)\vartheta_{n_1}(k_{\mathrm{cf}} - k_{n_1})}{(m - 1)k_{\mathrm{cf}} + k_{n_1} + \vartheta_{n_1}(k_{\mathrm{cf}} - k_{n_1})}. \tag{20}$$

Al_2O_3 and Cu nanoparticles are denoted by n_1 and n_2, respectively, while cf and *hf* denote carrier and hybrid fluid, respectively. The hybrid nanofluid is developed by combining two types of nanoparticles, alumina and copper dispersed in the transfer fluid. The symbol represents the proportion of the total volume that this mixture makes up.

3 Methodology

Assuming that A and B are constants, then $x \in [A, B]$, the ith Haar wavelet family is defined as

$$H_i(x) = \begin{cases} 1 & \text{for} \quad x \in [a_1, b_1) \\ -1 & \text{for} \quad x \in [b_1, c_1) \\ 0 & \text{elsewhere,} \end{cases} \tag{21}$$

with

$$a_1 = k/m_1, \quad b_1 = k + 1/2/m_1, \quad c_1 = k + 1/m_1, \tag{22}$$

where $m_1 = 2^j$ is the highest attainable resolution. We will refer to this quantity as $M = 2j$, each of the $2M$ subintervals of the interval $[A, B]$ has a length $x = (B, A)/2M$, where M is the number of subintervals $(2M)$, a translation parameter $k = 0, 1, \ldots, m_1 - 1$, and a dilatation parameter $j = 0, 1, \ldots J$. The formula for the wavelet number i is $i = m_1 + k + 1$.

For the Haar function and their integrals,

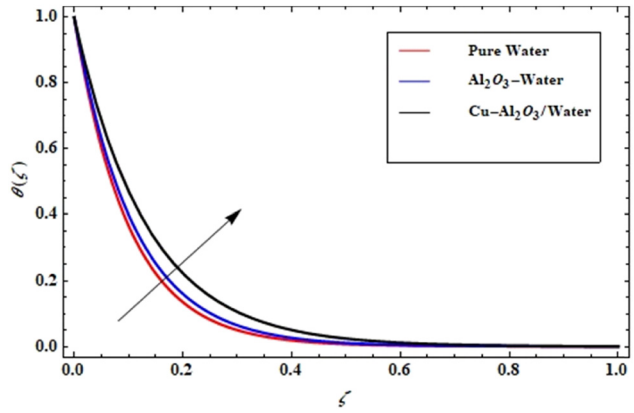

Figure 3: Particle concentration *versus* $\theta(\zeta)$.

$$p_{i1}(x) = \int_0^x H_i(\bar{x}), \tag{23}$$

$$p_{i,\,l+1}(x) = \int_0^x p_{i,l}(\bar{x})\mathrm{d}\bar{x}, \quad l = 1, 2, \ldots.$$

To calculate these integrals, we use Eq. (21):

$$p_{i1}(x) = \begin{cases} x - a_1 & \text{for} \quad x \in [a_1, b_1) \\ c_1 - x & \text{for} \quad x \in [b_1, c_1) \\ 0 & \text{elsewhere,} \end{cases} \tag{24}$$

$$p_{i2}(x) = \begin{cases} \dfrac{1}{2}(x - a_1)^2 & \text{for} \quad x \in [a_1, b_1) \\ \dfrac{1}{4m_1{}^2} - \dfrac{1}{2}(c_1 - x)^2 & \text{for} \quad x \in [b_1, c_1) \\ \dfrac{1}{4m_1{}^2} & \text{for} \quad x \in [c_1, 1) \\ 0 & \text{elsewhere,} \end{cases} \tag{25}$$

$$p_{i3}(x) = \begin{cases} \dfrac{1}{6}(x - a_1)^3 & \text{for} \quad x \in [a_1, b_1) \\ \dfrac{1}{4m_1{}^2}(x - b_1) - \dfrac{1}{6}(c_1 - x)^3 & \text{for} \quad x \in [b_1, c_1) \\ \dfrac{1}{4m_1{}^2}(x - \beta) & \text{for} \quad x \in [c_1, 1) \\ 0 & \text{elsewhere.} \end{cases} \tag{26}$$

We also present the following notation:

$$C_{i1} = \int_0^L p_{i1}(\bar{x})\mathrm{d}\bar{x}, \tag{27}$$

$$C_{i2} = \int_0^L H_i(\bar{x})\mathrm{d}\bar{x}. \tag{28}$$

Summation of the Haar wavelet function can be written as

$$f(x) = \sum_{i=1}^{\infty} a_i H_i(x). \tag{29}$$

Using wavelets, we may approximate the highest order derivatives of f and θ given by problems (10) and (11) to build a straightforward and precise Haar wavelet collocation method:

$$f'''(\zeta) = \sum_{i=1}^{2M} a_i H_i(\zeta), \tag{30}$$

$$\theta''(\zeta) = \sum_{i=1}^{2M} b_i H_i(\zeta). \tag{31}$$

Integrating Eq. (30), we obtain the values $f'''(\zeta) f''(\zeta)$, $f'(\zeta)$ and $f(\zeta)$, respectively,

$$f'''(\zeta) = \sum_{i=1}^{2M} a_i \left(p_{i,1}(\zeta) - \frac{1}{L} C_{i,1} \right), \tag{32}$$

$$f''(\zeta) = \sum_{i=1}^{2M} a_i \left(p_{i,2}(\zeta) - \frac{1}{L} \zeta C_{i,1} \right), \tag{33}$$

$$f'(\zeta) = \sum_{i=1}^{2M} a_i \left(p_{i,3}(\zeta) - \frac{1}{L} \frac{\zeta^2}{2} C_{i,1} \right), \tag{34}$$

$$f(\zeta) = \sum_{i=1}^{2M} a_i \left(p_{i,4}(\zeta) - \frac{1}{L} \frac{\zeta^3}{3} C_{i,1} \right). \tag{35}$$

Assume L is a large number. A numerical solution for the ordinary differential equations (ODEs) is obtained by substituting Eqs. (30)–(35) into Eqs. (10) and (11). In the next section, we can see a visual representation of the results of the proposed solution.

4 Results and discussions

The study of the thermal conductivity properties of a hybrid nanofluid and the influence of the Lorentz force on a three-dimensional stretched surface have significant practical applications in several industrial sectors. The potential of this discovery to revolutionize energy-intensive processes, such as heat exchangers in HVAC systems and industrial applications, lies in its ability to enhance heat transfer efficiency. Consequently, it can result in substantial energy conservation and a diminished environmental impact. Furthermore, it possesses the capacity to improve the effectiveness of cooling systems for electrical devices, hence extending their longevity and maximizing their efficiency. Moreover, it can play a pivotal role in the advancement of renewable energy technology, aviation applications, and biomedical devices. The findings also have practical applications in the domains of materials

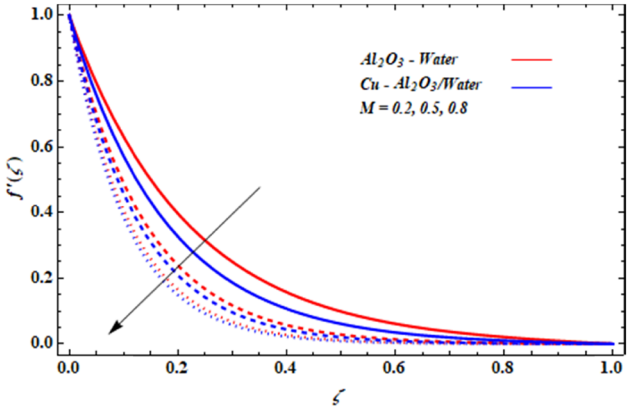

Figure 4: Effect of M on $f'(\zeta)$.

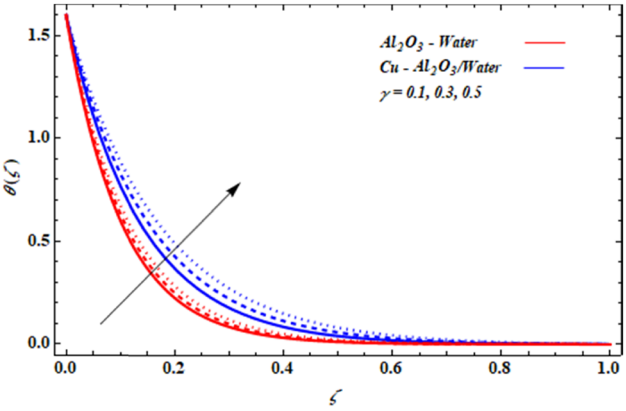

Figure 6: Effect of λ on $f'(\zeta)$.

processing and manufacturing, resulting in improved material properties and conservation of resources, while simultaneously decreasing thermal emissions for a more sustainable future.

Distribution patterns of velocity and temperature for the Al_2O_3/H_2O and $Cu–Al_2O_3/H_2O$ and the base fluid water are depicted in Figures 2 and 3, respectively. Because of their unique physical features, the velocity and temperature lines of these fluids appear to be displayed differently in these diagrams. As shown in Figure 2, our research shows that the hybrid nanomaterial significantly decreases the velocity profile in comparison to the dispersion of alumina nanoparticles. This indicates an enhanced ability to control the flow. Furthermore, Figure 3 demonstrates that the inclusion of alumina nanoparticles improves the temperature distribution of water. Moreover, when mixed with the hybrid nanomaterial, this enhancement is further intensified, suggesting its capacity to greatly enhance heat transfer efficiency.

The effect of the magnetic field strength M on $f'(\zeta)$ and $\theta(\zeta)$ of the nanofluid and the multiphase nanocomposite fluid is shown in Figures 4 and 5. Figure 4 clearly illustrates the impact of the magnetic parameter on the velocity profiles. As the magnetic parameter is increased, the velocity profiles exhibit a significant decrease, which can be attributed to the increasing Lorentz force produced by the applied magnetic field.

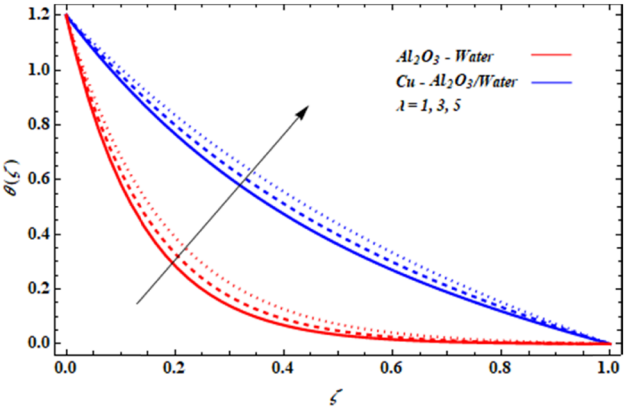

Figure 7: Effect of λ on $\theta(\zeta)$.

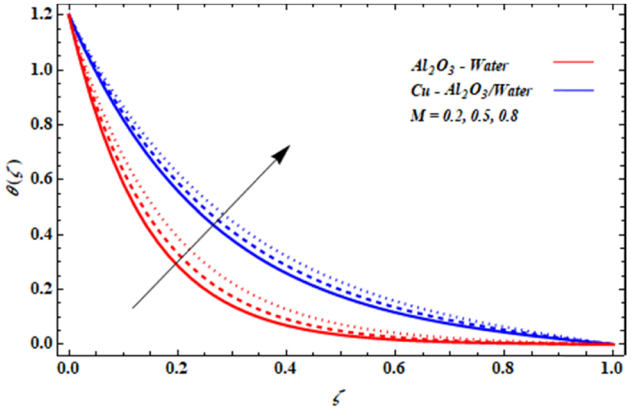

Figure 5: Effect of M on $\theta(\zeta)$.

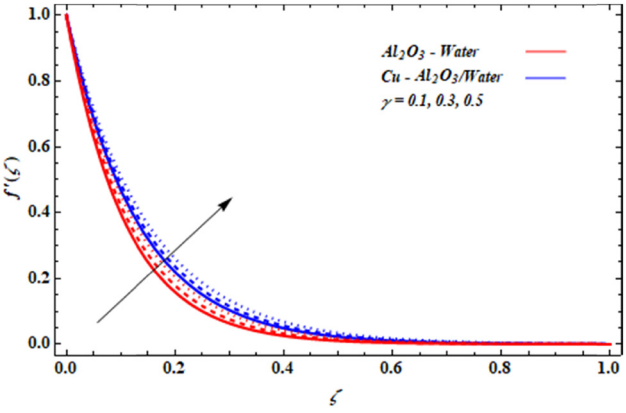

Figure 8: Effect of γ on $f'(\zeta)$.

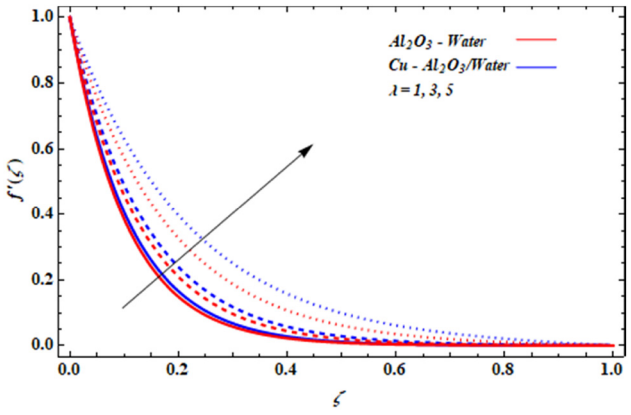

Figure 9: Effect of γ on $\theta(\zeta)$.

The effect of the magnetic parameter M on $\theta(\zeta)$ of the nanofluid and the multiphase nanocomposite fluid is shown in Figure 5. The frictional force between fluid layers increases as the magnetic parameter increases, leading to more extreme temperature distributions.

Both the velocity and temperature distributions of a nanofluid and a hybrid nanofluid are shown to be affected by λ (Figures 6 and 7). We are increasing the λ yields to improve velocity and temperature distributions.

Figures 8 and 9 show the relationship between the curvature parameter γ and the temperature and velocity distribution of nanofluids and hybrid nanofluids, respectively. A higher curvature parameter value results in better velocity and temperature distributions.

Figure 10 depicts the influence of the radiation parameter Rd on the heat transfer, denoted by $\theta(\zeta)$, in both nanofluids and hybrid nanofluids. As the radiation parameter Rd increases, the temperature profiles for both nanofluids and mixed nanofluids also increase. Nevertheless, it is important to mention that the temperature increase is more significant in the hybrid nanofluid, suggesting its improved capacity to capture and control heat when exposed to radiation.

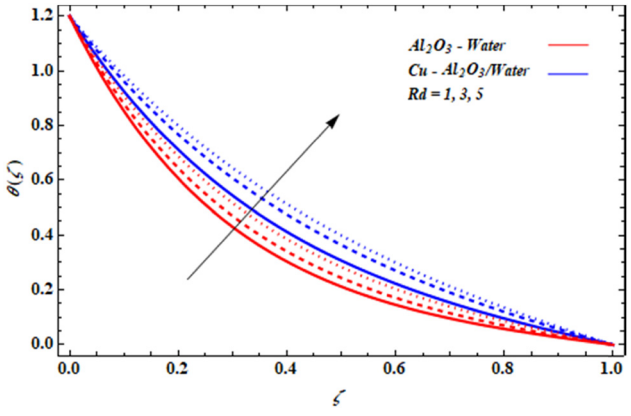

Figure 10: Effect of Rd on $\theta(\zeta)$.

5 Conclusion

This article discusses how a hybrid nanofluid of alumina and copper/water improves heat transmission and fluid flow properties as it flows past a stretched cylinder. The effects of an external magnetic field are also considered. Nonlinear ODEs with appropriate boundary conditions constitute the subsequent flow issue, in which similarity transformations reduce to a non-dimensional form. We can see how different factors affect the velocity and temperature characteristics. The most important results are as follows:

- The temperature profile of a hybrid nanofluid improves when the impact M is increased while the $f'(\zeta)$ decreases.
- The velocity and temperature distribution profiles benefited from an increase in the convection λ and curvature parameters γ.
- The presence of the hybrid material increases the convective heat transfer, which is at its lowest for the copper/water nanofluid.

Acknowledgments: The authors acknowledge Princess Nourah bint Abdulrahman University Researchers Supporting Project (number PNURSP2023R183), Princess Nourah bint Abdulrahman University, Riyadh, Saudi Arabia. This work was supported by the Deanship of Scientific Research, the Vice Presidency for Graduate Studies and Scientific Research, King Faisal University, Saudi Arabia (Grant No. 4716).

Funding information: Princess Nourah bint Abdulrahman University Researchers Supporting Project (number PNURSP2023R183), Princess Nourah bint Abdulrahman University, Riyadh, Saudi Arabia. This work was supported by the Deanship of Scientific Research, the Vice Presidency for Graduate Studies and Scientific Research, King Faisal University, Saudi Arabia (Grant No. 4716).

Author contributions: All authors have accepted responsibility for the entire content of this manuscript and approved its submission.

Conflict of interest: The authors state no conflict of interest.

Data availability statement: All data generated or analyzed during this study are included in this published article.

References

[1] Li Z, Wang K, Li W, Yan S, Chen F, Peng S. Analysis of surface pressure pulsation characteristics of centrifugal pump magnetic liquid sealing film. Front Energy Res. 2022;10:937299. doi: 10.3389/fenrg.2022.937299.

[2] Kong L, Liu G. Synchrotron-based infrared microspectroscopy under high pressure: An introduction. Matter RadiExtremes. 2021;6(6):68202. doi: 10.1063/5.0071856.

[3] Zhang G, Chen J, Zhang Z, Sun M, Yu Y, Wang J, et al. A novel parametric model for nonlinear hysteretic behaviours with strain-stiffening of magnetorheological gel composite. Composite Struct. 2023;318:117082. doi: 1016/j.compstruct.2023.117082.

[4] Sun L, Liang T, Zhang C, Chen J. The rheological performance of shear-thickening fluids based on carbon fiber and silica nanocomposite. Phys Fluids. 2023;35(3):32002. doi: 10.1063/5.0138294.

[5] Jia L, Wang Z, Wang L, Zeng J, Du P, Yue Y, et al. Self-standing boron nitride bulks enabled by liquid metal for thermal management. Mater Horiz. 2023. doi: 10.1039/D3MH01359F.

[6] Kuang W, Wang H, Li X, Zhang J, Zhou Q, Zhao Y. Application of the thermodynamic extremal principle to diffusion-controlled phase transformations in Fe-C-X alloys: Modeling and applications. Acta Materialia. 2018;159:16–30. doi: 1016/j.actamat.2018.08.008.

[7] Chen L, Zhao Y. From classical thermodynamics to phase-field method. Prog Mater Sci. 2022;124:100868. doi: 1016/j.pmatsci.2021.100868.

[8] Bhatti MM, Rashidi MM. Effects of thermo-diffusion and thermal radiation on Williamson nanofluid over a porous shrinking/stretching sheet. J Mol Liq. 2016;221:567–73.

[9] Bhatti MM, Abbas T, Rashidi MM. Effects of thermal radiation and electromagnetohydrodynamics on viscous nanofluid through a Riga plate. Multidiscip Model Mater Struct. 2016;12:605–18.

[10] Shirvan KM, Mamourian M, Mirzakhanlari S, Ellahi R. Numerical investigation of heat exchanger effectiveness in a double pipe heat exchanger filled with a nanofluid: a sensitivity analysis by response surface methodology. Powder Technol. 2017;313:99–111.

[11] Shirvan KM, Ellahi R, Mamourian M, Moghiman M. Effects of wavy surface characteristics on natural convection heat transfer in a cosine corrugated square cavity filled with nanofluid. Int J Heat Mass Transf. 2017;107:1110–8.

[12] Chamkha AJ, Rashad AM. Natural convection from a vertical permeable cone in a nanofluid saturated porous media for uniform heat and nanoparticles volume fraction fluxes. Int J Numer Methods Heat Fluid Flow. 2012 Oct 26;22(8):1073–85.

[13] Chamkha A, Gorla RS, Ghodeswar K. Non-similar solution for natural convective boundary layer flow over a sphere embedded in a non-Darcy porous medium saturated with a nanofluid. Int J Microscale Nanoscale Therm Fluid Transp Phenom. 2011 Apr 1;2(2):135.

[14] Chamkha AJ, Issa C, Khanafer K. Natural convection from an inclined plate embedded in a variable porosity porous medium due to solar radiation. Int J Therm. 2022;41(1):73–81.

[15] Chamkha AJ. Coupled heat and mass transfer by natural convection about a truncated cone in the presence of magnetic field and radiation effects. Numer Heat Transfer: Part A: Appl. 2001 Apr;39(5):511–30.

[16] Suresh S, Venkitaraj KP, Selvakumar P, Chandrasekar M. Synthesis of Al_2O_3–Cu/hybrid water nanofluids using two-step method and its thermo physical properties. Colloids Surf A. 2011;388:41–8.

[17] Suresh S, Venkitaraj KP, Selvakumar P, Chandrasekar M. Effect of Al_2O_3–Cu/water hybrid nanofluid in heat transfer. Exp Therm Fluid Sci. 2012;38:54–60.

[18] Suresh S, Venkitaraj KP, Hameed MS, Sarangan J. Turbulent heat transfer and pressure drop characteristics of dilute water-based Al_2O_3–Cu hybrid nanofluids. J Nanosci Nanotechnol. 2014;14:2563–72.

[19] Momin GG. Experimental investigation of mixed convection with water-Al_2O_3 & hybrid nanofluid in an inclined tube for laminar flow. Int J Sci Technol Res. 2013;2:195–202.

[20] Askari S, Koolivand H, Pourkhalil M, Lotfi R, Rashidi A. Investigation of Fe_3O_4/Graphene nanohybrid heat transfer properties: an experimental approach. Int Commun Heat Mass Transf. 2017;87:30–9.

[21] Mehryan SA, Kashkooli FM, Ghalambaz M, Chamkha AJ. Free convection of hybrid Al_2O_3–Cu water nanofluid in a differentially heated porous cavity. Adv Powder Technol. 2017;28:2295–305.

[22] Benzema M, Benkahla YK, Labsi N, Ouyahia S-E, El Ganaoui M. Second law analysis of MHD mixed convection heat transfer in an irregular vented cavity filled with Ag-MgO/water hybrid nanofluid. J Therm Anal Calorim. 2019;137:1113–32.

[23] Sundar LS, Sharma KV, Singh MK, Sousa AC. Hybrid nanofluids preparation, thermal properties, heat transfer and friction factor a review. Renew Sustain Energy Rev. 2017;68:185–98.

[24] Labib MN, Nine MJ, Afrianto H, Chung H, Jeong H. Numerical investigation on base fluids and hybrid nanofluid effect in forced convective heat transfer. Int J Therm Sci. 2013;71:163–71.

[25] Abbas N, Shatanawi W, Abodayeh K. Computational analysis of MHD nonlinear radiation casson hybrid nanofluid flow at vertical stretching sheet. Symmetry. 2022 Jul;14(7):1494.

[26] Abbas N, Shatanawi W. Heat and mass transfer of micropolar-casson nanofluid over vertical variable stretching riga sheet. Energies. 2022 Jul;15(14):4945.

[27] Shatnawi TA, Abbas N, Shatanawi W. Comparative study of Casson hybrid nanofluid models with induced magnetic radiative flow over a vertical permeable exponentially stretching sheet. AIMS Math. 2022 Jan;7(12):20545–64.

[28] Shatnawi TA, Abbas N, Shatanawi W. Mathematical analysis of unsteady stagnation point flow of radiative Casson hybrid nanofluid flow over a vertical Riga sheet. Mathematics. 2022 Sep;10(19):3573.

[29] Abbas N, Shatanawi W. Theoretical survey of time-dependent micropolar nanofluid flow over a linear curved stretching surface. Symmetry. 2022 Aug;14(8):1629.

[30] Lepik U. Haar wavelet method for nonlinear integrodifferential equations. Appl Math Comput. 2006;176:324–33.

[31] Lepik U. Numerical solution of evolution equations by the Haar wavelet method. Appl Math Comput. 2007;185:695–704.

[32] Šarler B, Aziz I. Haar wavelet collocation method for the numerical solution of boundary layer fluid flow problems. Therm Sci. 2011;50:686–97.

[33] Yasmin H, Aljahdaly NH, Saeed AM, Shah R. Probing families of optical soliton solutions in fractional perturbed Radhakrishnan–Kundu–Lakshmanan model with improved versions of extended direct algebraic method. Fractal Fract. 2023;7(7):512.

[34] Yasmin H, Aljahdaly NH, Saeed AM, Shah R. Investigating families of soliton solutions for the complex structured coupled fractional biswas–arshed model in birefringent fibers using a novel analytical technique. Fractal Fract. 2023;7(7):491.
[35] Yasmin H, Aljahdaly NH, Saeed AM. Investigating symmetric soliton solutions for the fractional coupled konno–onno system using improved versions of a novel analytical technique. Mathematics. 2023;11(12):2686.
[36] Alshehry AS, Ghani F, Shah R, Nonlaopon K. Comparative analysis of advection–dispersion equations with Atangana–Baleanu fractional derivative. Symmetry. 2023;15(4):819.
[37] Zidan AM, Khan A, Alaoui MK, Weera W. Evaluation of time-fractional Fisher's equations with the help of analytical methods. Aims Math. 2022;7(10):18746–66.
[38] Mukhtar S, Noor S. The numerical investigation of a fractional-order multi-dimensional Model of Navier–Stokes equation *via* novel techniques. Symmetry. 2022;14(6):1102.